Velocity estimation of thunderstorm movement and dealiasing of single Doppler radar during convective events

Ioannis Samos[1,2] · Helena Flocas[1] · Petroula Louka[3] · Flora Gofa[2] · Antonios Emmanouil[2]

Abstract

The use of meteorological radars in monitoring current weather conditions is crucial regarding the observation of the evolution and dissipation of thunderstorms. Thus, Doppler velocities being measured in each radar scan and velocity vectors derived from Numerical Weather Prediction (NWP) models—that are usually not as highly resolving as radar scans—are combined, as a monitoring utility during the evolution of a convective weather event. The objective of this study is to develop a new method that allows the implementation of a thunderstorm movement velocity estimation technique combining block matching and optical flow techniques. This new method constitutes a nowcasting (NWC) application that enables the use of a single Doppler radar without the need of using NWPs. The method relies on the estimation of the thunderstorm movement vector velocities (Doppler velocity) for each constant altitude plan position indicator (CAPPI) and through correction for aliasing errors to obtain 3D vector velocity fields for convective systems. The performance of the method is evaluated for selected case studies of convective thunderstorms under different synoptic scale conditions over Greece, a geographical area with challenges in forecasting due to its sharp relief and the need for optimization of the use of radar products.

Introduction

The accurate estimation of thunderstorm movement is very useful information for short-term forecasting in meteorology, known as nowcasting, as it poses a challenge for many Meteorological Services to acquire a valid short forecast for the affected areas. The three-dimensional wind vector, that determines the evolution of a thunderstorm, is one of the most fundamental variables in describing the state of the atmosphere (Sawyer 1977; Nair 2022) and it is usually

✉ Ioannis Samos
   ioannis.samos@phys.uoa.gr

1 Section of Environmental Physics and Meteorology, Department of Physics, National and Kapodistrian University of Athens, 15772 Athens, Greece

2 Hellenic National Meteorological Service, 16777 Hellinikon, Athens, Greece

3 Department of Mathematics and Natural Sciences, Hellenic Air Force Academy, 13672 Acharnes, Greece

measured by remote sensors, such as ground-based radars. Moreover, lightning activity is a strong indication of convective weather, although, the usage of lightning data does not provide information on the future path or the evolution of a thunderstorm.

The most valuable parameter of thunderstorm movement estimation is the Doppler velocity, as derived from weather radars, which is the velocity component in the direction of the radar beam. Single-Doppler radar observations provide only one component of the velocity, which is the radial Doppler velocity. However, in order to fully comprehend the evolution of a convective weather system, it is essential to estimate all three components of wind vectors. Existing techniques in the literature for wind estimation are based on various properties of radar data:

a. The VAD (Velocity Azimuth Display) technique (Browning and Wexler 1968; Waldteufel and Corbin 1979; Liang 2007) comprises the retrieval of 3D-vector velocities under the assumption that the horizontal wind field at a given altitude varies linearly with distance along each ray of the radar scan within the regions scanned. The radial wind data are then fitted to a sinu-

soidal curve, as a function of azimuth for fixed elevations. The VAD technique can retrieve the mean wind within a given range of radar scan, which is a full 360° sweep scan, based on the linearity assumption. The above assumption unavoidably leads to uniform wind vectors that all have the same direction and magnitude, even in distances far from the site of the radar and cannot produce a grid of vectors.

b. The UW (Uniform Wind) technique (Persson 1987; Liang 2007) assumes that the wind is uniform in a limited user-defined region, e.g., 30° sweep scan, which again does not provide adequate representation of the wind field (Liang 2007).

c. The Velocity Azimuth Process (VAP) technique uses the same assumption as UW technique regarding wind and uniform characteristics, which means that the horizontal wind vectors of two neighboring azimuths are uniform (Tao 1992; Liang 2007).

Both UW and VAP can be utilized to retrieve detailed wind vectors in a gridded format but they cannot be used for radar elevation scans in which the elevation of the antenna is significant enough. The effects of fall velocity and elevation angle could only be neglected in low elevation scans. In both UW and VAP techniques, the mean wind in a limited region can be retrieved, since these techniques obtain higher resolution than VAD. In general, velocity vectors from all three techniques normally smooth out the wind field and are not suitable for convective scale wind estimates, especially if the grid resolution is below 4 km (Luo et al. 2014). These techniques may be used for a first estimation of large-scale or mesoscale winds and need radial scan of Doppler winds to retrieve information regarding present and future weather situation when isolated thunderstorms are present.

Accurate data are essential for effective monitoring thunderstorms. This is a challenge for many Meteorological Services, especially when outdated radar equipment is used. This happens because it produces noisy returns that need to be further processed. Furthermore, operational configuration of Doppler radars by many authorities is usually based on small pulse repetition frequencies (PRF's), which can result in sine folding and aliasing even at low Doppler velocities. Therefore, for Doppler velocity estimation at local and convective scale, velocity dealiasing processes are suggested (Li and Wei 2010; Liang 2019). Usually, a proposed subpixel motion estimation of both direction and horizontal velocity without interpolation is used (Chan et al. 2010), that treats isolated convective radar returns in dBz as sequential images. The feasibility of this dealiasing technique applied in this paper refers to the use of radars regarding thunderstorm tracking or weather evolution from Meteorological Services where convective systems are followed by extreme precipitation and wind (Wan 2021;

Cassola 2023), as well as during forecast simulations, covering aspects of assimilation processes of radar data (Liu 2021; Sugimoto et al. 2009; Gastaldo 2018). With respect to data assimilation, as Numerical Weather Prediction (NWP) forecasts are based on updating forecasted fields from the latest observations, this technique will improve the wind vector information after filtering dBz signal and dealiasing Doppler velocities. Many real-time forecasting systems depend on running alone high-resolution NWP models on supercomputers with high-computational cost (Honda et al. 2022). The combination of these data with NWP information may provide high-resolution wind field data for further uses by the Meteorological Services.

The main objective of this study is to develop and evaluate a new method that estimates more precisely convective vertical velocity by combining the calculated thunderstorm movement horizontal vector velocities from an algorithm, that employs radar output Doppler velocities. This combination is used to acquire a hybrid vector that can be considered as the vertical component of the wind vector. Finally, an additional objective of this study is to suggest a methodology to overcome the sine folding of Doppler radar velocities by dealiasing through algorithms as well as filtering of data.

Radar data and adaptations

This study employs Doppler radar data, including reflectivity (in dBz) and Doppler velocities. In this section, radar data characteristics are presented in "Radar data characteristics" section, followed by the description of dealiasing and filtering of radar data in "Radar dealiasing and filtering" section, which are the required adaptations for the final output to be delivered, which are horizontal and vertical velocities.

Radar data characteristics

Regarding the technical characteristics, the Ymittos radar is a C band (5.61 GHz) Doppler weather radar located at latitude 37.946°N and longitude 23.814°E, providing twelve (12) elevation Plan Position Indicator (PPI) scans, with a horizontal resolution of 400 m. The Larissa radar is an S band (2.708 GHz) Doppler weather radar located at latitude 39.6446°N and longitude 22.4603°E, providing twelve (12) elevation PPI scans, with a horizontal resolution of 150 m. The Thessaloniki radar is a S band (2.816 GHz) Doppler weather radar located at latitude 40.5282°N and longitude 22.9757°E, providing twelve (12) elevation PPI scans, with a horizontal resolution of 150 m. The operational visibility of scans for all radars, which represents the maximum scanning radius under ideal conditions, is 300 km. Reliable data collection and operational factors limit the scan radius to
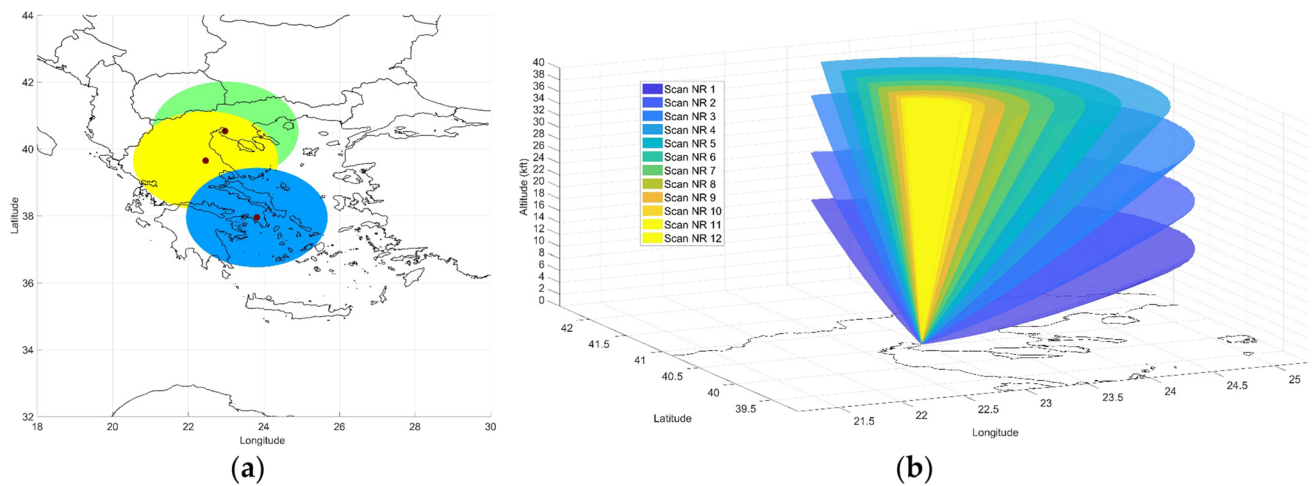
Fig. 1 **a** Implemented Greek radar network coverage of Ymittos (blue), Larissa (yellow) and Thessaloniki (green) sites and **b** Three-dimensional representation of radar scan from Thessaloniki radar for all elevation angles

170 km (Fig. 1a) for all radars used, which is considered as the effective visibility. An example of the radar scan for all elevation angles is provided in Fig. 1b. Each scan at every elevation angle is presented as a solid surface, instead of a volume, showing the conus areas covered by the radar. In every calculation earth curvature correction has been applied. Each elevation angle is represented by a color in Fig. 1b. The sum of all elevation angle scans forms a three-dimensional area of the atmosphere.

The radar reflectivity factor Z (Šaur 2021) is calculated as the maximum value on each pixel between the selected heights of the volume scan. Since all radars are based on the Doppler effect to calculate Doppler velocities, the velocity of meteorological targets is easily measured by the radial velocity. Radial velocity is the measure of the target motion toward or away from the radar. In addition to the radar's internal filtering process, an additional noise filtering algorithm was used to analyze the radar readings and filter the radial velocity. However, various artifacts can still appear in radar data fields in several forms of noise (Divjak 1999).

Radar dealiasing and filtering

When the radar antenna rotates at a fixed elevation angle, the output values of Doppler velocities are a function of azimuth (Battan 1973). In this section, the physical background regarding data aliasing of Doppler wind retrieval is presented. This is a significant problem since the acquired values of Doppler velocity measurements have been altered due to sine folding.

For a Doppler radar operating at a specific wavelength, the product of Vmax and rmax is constant, implying that when rmax increases, Vmax decreases and vice versa. This unfortunate tradeoff between Vmax and rmax is frequently referred to as the "Doppler dilemma" (Rinehart 2004). However, spatial continuity permits one to readily identify visually the presence of aliasing and make proper adjustments. Computer algorithms are designed to objectively identify and correct aliased Doppler velocity data (Eilts and Smith 1990). Such an algorithm is described in the next section.

A dealiasing method is employed, assuming uniformly distributed derivative along the distance of each ray of the radar scan. This algorithm is employed for each elevation angle solely, starting from the top downwards to the one closest to the ground. For each elevation angle, the data form a 2D grid, where the x-axis represents the azimuth (rotating angle—i points) and the y-axis represents the distance from the radar center (j points). For every j, a set of points is derived that should follow a sinusoidal curve (not shown). To determine the amplitude and phase of the sine curve, a range of sine curves with a step of 10° per azimuth and 5 m/s per amplitude is calculated and folded following a Doppler radar, by means of the maximum speed of all scans. Then, the set of calculated folded sine curves is subtracted one by one from the original folded sine, and a matrix of subtractions is formed. The lowest of the absolute values of this matrix corresponds to the values of amplitude and phase, which are close to the original observed value. Therefore, for every j, a phase chart represents the wind direction of Doppler velocities. A known bug in the algorithm is that a sine with phase 0° and 180° appears two minima, since the absolute value is used for the calculations. As a result, the above-mentioned chart can present points with difference of 180 in the wind direction. Similarly, the fast Fourier transformation (FFT) can provide the wind direction; however, it is insufficient and misleading toward the calculation of the phase of the sines, providing further erroneous amplitudes in areas where Doppler winds exist (not shown).
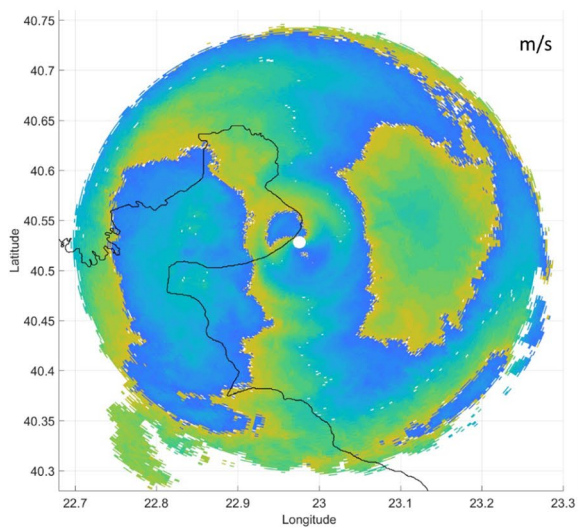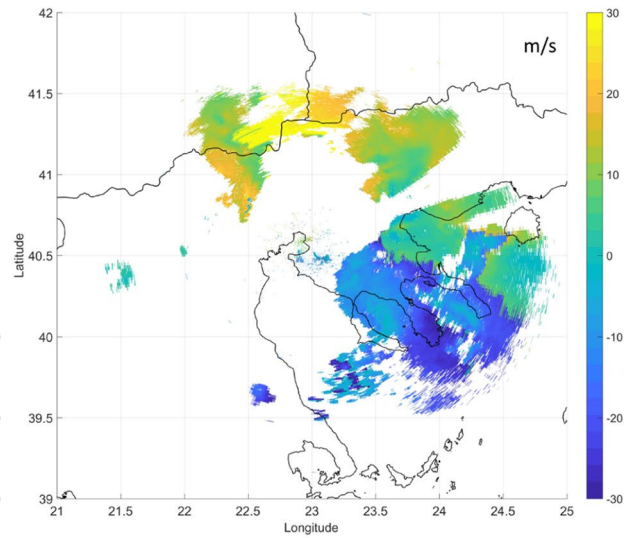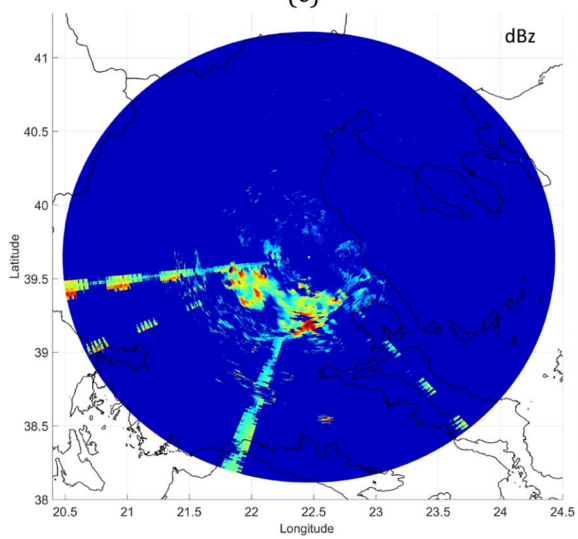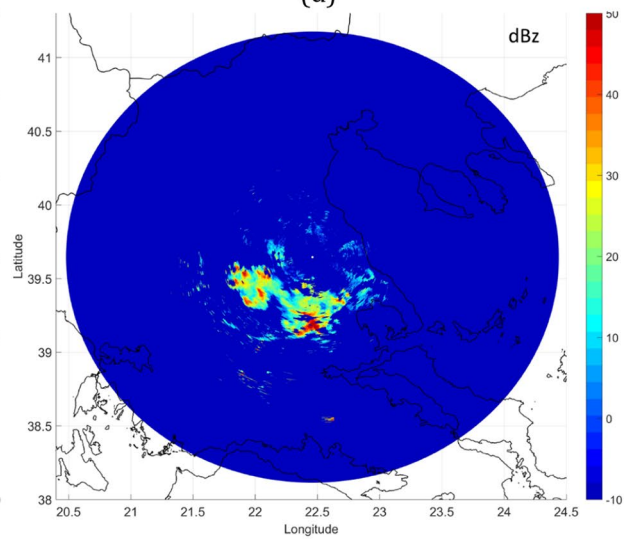
(a)
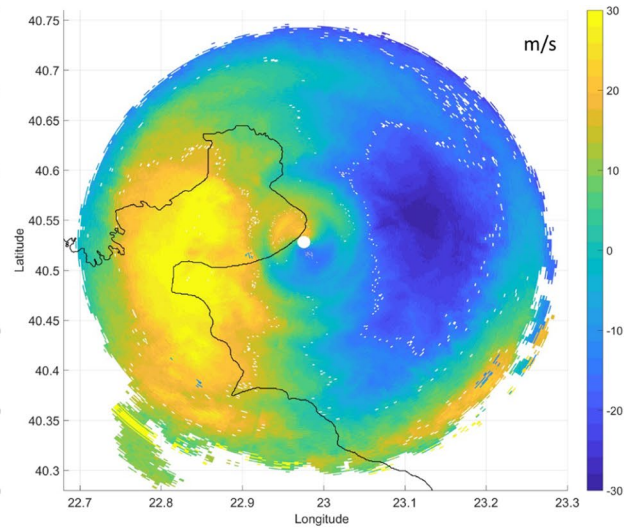
(b)
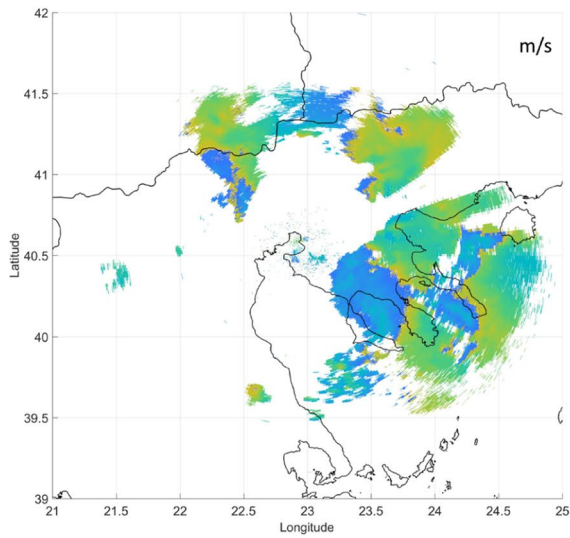
(c)

(d)

(e)

(f)

Fig. 2 Thessaloniki radar Doppler velocity plot **a** aliased velocities of Vmax equal to 15.92 m/s, **b** dealiased Doppler velocity based on methodology, **c** original aliased scan, **d** dealiased scan. Larissa radar dBz measurements **f** unfiltered scan and **g** after applying filtering algorithm

Having the horizontal vector velocities calculated in advance in 3D space, for each elevation angle the correct phase of the wind direction is assigned. Once calculated, the Doppler scan is unfolded by the algorithm, based on the wind direction calculated for each j. This time the step of azimuth is reduced to 1 degree and the amplitude to 0.1 m/s. The algorithm for every elevation angle results in a full dealiased set of observations (Fig. 2a), enabling the interpolation of Doppler velocities, from polar to Cartesian coordinates, and allows the use of dealiased Doppler velocities in data assimilation (Sugimoto et al. 2009; Gastaldo 2018).

This methodology of dealiasing employed in this study is subject to certain limitations. Specifically, it necessitates enough data points to be available at a full 360° range, ideally without any missing data between them. As such (Fig. 2c), it may not be applicable for analyzing individual thunderstorms due to a lack of available data points in certain locations (Fig. 2d).

Thunderstorms that possess a compact structure and are characterized by limited spatial extent pose a significant challenge for the application of this algorithm and, consequently this algorithm cannot be employed to dealiase the data (Fig. 2b).

Fortunately, isolated thunderstorms have low horizontal velocities within the Nyquist cointerval and usually have no need to be dealiased.

Low elevation radar scans contain clutter, both on dBz values as well as in Doppler velocity, especially the ones with old technology. A simple convolution algorithm eliminates single rays of clutter. The pattern is often the same, due to physical obstacles (e.g., mountains) or radio wave interference. In Fig. 2e, a ray of clutter exists, with no Doppler velocities (not shown), and no dBz values along its axis, either on its left or on its right. The convolution algorithm treats radar data of each elevation scan as a two-dimensional matrix, and for every single point of the matrix, it performs calculation by recognizing around it the remaining eight points of a 3×3 matrix. If the point registers a dBz value, then to this point is assigned the number 1. If it does not register a dBz value, the number 0 is assigned to it. The algorithm, then, sums up the number of dBz cells and the highest value can be 9, meaning that all the surrounding points have dBz values—valid, while the lowest can be 0, meaning that no surrounding point has dBz values (non-valid—clutter). The resulting matrix is used as a reference for determining clutter cells in the original matrix.

Values of the reference matrix higher than 5 are considered to be valid. This threshold value is derived empirically from filtering the low level scans of all radars used in this paper. It was found that values less than 4 do not eliminate sufficiently low level clutter, while values higher than 5 eliminate more clutters and compromise the integrity of the produced matrix of values (Fig. 2f). The linear interpolation performed in each CAPPI, after using value 5 for filtering, has no significant impact on the resulted matrix of values, since the filtered values are treated as NaN's (Not A Number). The filtering process applied at every elevation angle produces a complete set of dealiased observations, enabling the utilization of dealiased reflectivity data (dBZ) for data assimilation purposes (Sugimoto et al. 2009).

Methodology

The methodology employed in this study consists of sequential steps that provide the vertical velocity field as a final product, as well as intermediate steps for acquiring horizontal velocity components with the aid of MATLAB software version 2019b (*MathWorks—Makers of MATLAB and Simulink*, n.d.) (https://www.mathworks.com). Other techniques for horizontal wind retrieval such as VAD, VAP and UW have their limitations as mentioned in the introductory section. In addition, NWP forecasts can provide high-resolution information on the horizontal and vertical components of the atmospheric wind field (Nolan et al. 2021; Skolnik 2008). In order to evaluate the relative advantage of the proposed method in the estimation of the movement of a thunderstorm, horizontal wind components are also calculated from the NWP model Weather Research and Forecasting-Advanced Research core model (WRF-ARW) and the VAD technique in order to compare and evaluate more diversely the results of this new method. The VAD technique was selected based on its computational efficiency and ease of use relative to other methodologies. The employment of the model and the VAD technique will be performed for different weather systems, as it is described in "Evaluation of methodology—convective events" section.

Extraction of reflectivity fields

To obtain the 2-D reflectivity values at various levels in the atmosphere, several aspects must be taken into account. After the processes of dealiasing and filtering, certain elevation angles are taken under consideration for the three-dimension scan area to be processed, where the radar scanned the atmosphere, which varied from site to site. It should be noted that the elevation angles are common but not identical for all the radars used in this study. Constant Altitude Plan Position Indicators (CAPPI) are estimated by

interpolating observations, which derived from each radar scan at different heights. By binning the data in vertical surfaces, a three-dimensional volume is calculated. As a result, surfaces with thickness set to 1.000 ft. are calculated. Linear interpolation was selected for dBz measurements (second step), because of the relatively low-computational cost and mostly in an effort to avoid overfitting in high values of dBz for lost observations that cubic or spline methods could produce. The analysis of grid interpolation performed is 0.02°at each flight level, ranging from ground level to ~ 16.700 m (55.000 ft).

Horizontal velocity calculation of thunderstorm movement

The focus of this study is the estimation of all three components of the wind speed during the evolution of a thunderstorm. The calculation of the displacement of pixels along x- and y-axes of two sequential images produces a two-dimensional array of vectors. This array can be interpreted as the horizontal vector velocities, by issuing units between pixels of an image and geo-referenced coordinates appropriately. Dimensionless quantities of dBz measurements of Doppler radars are used to produce timestamped frames for this calculation. Horizontal thunderstorm movement vector velocities are estimated in Eq. (1) with the aid of the algorithm of (Chan et al. 2010):

$$[velocity] = \frac{[distance]}{[time]} = \frac{0.02 \text{ deg}}{15 \text{ min}} = \frac{\frac{0.02 \text{ deg}}{\text{meters per latitude} \times \frac{\text{meters}}{\text{degrees}}}}{15 \times 60 \text{ s}}.$$

(1)

By applying the estimated thunderstorm movement horizontal velocity to the measured Doppler velocity, a hybrid vector of vertical velocity can then be calculated and it is presented in the following section.

Hybrid Vertical Wind vector estimation

The value of the radial velocity V_D (positive moving away from the radar and negative when moving toward) is observed at fixed range and elevation and can be expressed as (Tian et al. 2015):

$$V_D = W \times \sin \varphi + \cos \varphi \times (U \times \sin \theta + V \times \cos \theta),$$

(2)

where φ is the elevation angle, θ is the rotation angle along the x–y-axes and U and V are the Cartesian velocities measured in radar coordinates (r, θ). Having the results from Eq. (1) the horizontal components of the wind vector velocities (U and V) are estimated from the pixel displacement of sequential interpolated images in a Cartesian grid, derived from dimensionless quantities of dBz reflectivities. Following that, the measured Doppler radar

velocities (V_D) are combined with U and V to provide the W vertical component. Equation (2) is transformed (Tian et al. 2015), leading to the calculation of W:

$$W = \frac{\cos \varphi \times (U \times \sin \theta + V \times \cos \theta) - V_D}{\sin \varphi}.$$

(3)

NWP forecasts

In this study, WRF-ARW version 3.7.1 was employed (Powers-NCAR/UCAR 2008). For the simulation of the wind fields based on NWP forecasts, initial and boundary conditions were used from global forecasts of the IFS/ECMWF model. The data were retrieved for a region extending from 24°N to 64°N and from 30°W to 50°E. The simulated fields were available at hourly intervals on a 0.125° resolution area. The data were retrieved at pressure levels from 1000 to 50 hPa as well as on the model surface.

Diverse convective weather conditions are simulated, to utilize the results for any comparison performed. The initialization times of the simulations are selected to be close to the starting time of the convective events that were analyzed with the aid of model analyses available every six hours. The simulations were performed in a two-way nested configuration with two model domains—d01 and d02 (Fig. 3), all of which contained 50 vertical levels and whose horizontal grid spacing was 12 km and 4 km, respectively. The location of the innermost d02 domain was chosen to contain the full path of the observed thunderstorms, which is the Greek territory.

The WRF model includes options for different physical parameterizations, including microphysics, cumulus physics, surface physics, planetary boundary layer physics and radiation physics. The model performance is highly dependent on the parameterization schemes which might be suitable for one storm event but inappropriate for others. For this reason, the parameterization schemes remained fixed for the convective simulations that were analyzed. More specifically, the main physics packages used include the WRF Single-Moment 6-class (WSM6) microphysics scheme (Hong and Lim 2006), the new Kain–Fritsch cumulus parameterization scheme (Kain 2004), the Yonsei University planetary scheme for the planetary boundary layer (Hong et al. 2006) and the Rapid Radiative Transfer Model (RRTMG) shortwave and longwave radiation scheme (Dudhia 1989).

VAD application

VAD technique (Lee et al. 2014; Lim and Lee 2009; Tao 1992) requires a sinusoidal fitting of data. In case of aliased datasets (Fig. 2a, c, d, e), this is a very difficult task to achieve, since either discontinuities along radar sweeps or dealiasing

Fig. 3 Southeast Europe map over which the modeled Domain 1 (blue) and inner Domain 2 (yellow) used in the NWP applications
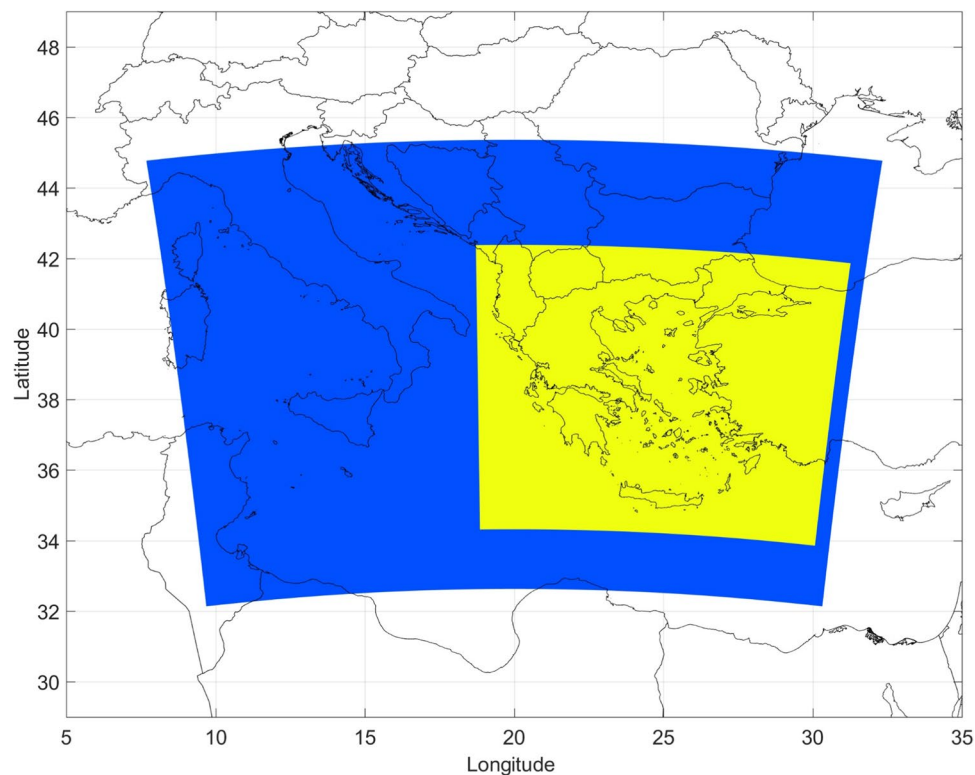
incapability could lead to non-valid wind estimates. A full radar sweep (360°) at the lowest elevation angle is usually set to a radius of 170 km. Having a step of 400 m sequential radar pulses for Ymittos radar, the resulting sinusoidal fits are 425, each of one representing the results at different locations along the radar radius. For elevations greater than the lowest, the results have specific heights as well. Each of the radar sweep data is fitted to produce VAD results, forming a three-dimensional array of velocities. Dealiased Doppler velocities are only fitted, and valid data are considered to have an RMSE greater than 75%. There are resulting fits that RMSE is very low (below 75%), and datasets are considered non-valid and consequently are neglected in this study. For a specific elevation angle and at a specific distance along a radar ray, Eq. (4) describes the wind derived by VAD technique (Liang 2007):

$$\bar{u} = \frac{\int_0^{2\pi} V_D \times \cos a \times da}{\int_0^{2\pi} V_D \times \cos^2 a \times da}, \tag{4}$$

where $\bar{u}$ is the calculated vector velocity magnitude, V_D is the Doppler velocity, and a is the azimuth angle.

Evaluation of methodology—convective events

Nowcasting applications require detailed forecasts of extreme weather phenomena such as thunderstorms. Wind field at various vertical levels is often associated with thunderstorm movement but there are cases when the wind field is not representative for the thunderstorm movement.

In this section, five test cases are presented where convective phenomena took place over Greek area, some of them with extreme thunderstorm intensity. The aim of this analysis is to evaluate the potential of the proposed methodology to calculate thunderstorm movement vectors of different convective systems and to compare them with ambient horizontal wind vectors as derived from WRF and VAD technique.

Necessary parts of the analysis that is performed for the various cases are included in the description of the cases. This includes the description of the synoptic characteristics of the weather event, presentation of the available NWP

forecasts, accompanied maximum dBz adapted data from available radar observations, estimation of the cross sections where convective phenomena occurred based on maximum dBz values, calculation and presentation of the vertical velocities based on these cross sections. Then, the 24-h precipitation amount based on IMERG data (Huffman et al. 2020) is used for validation of the thunderstorm movement path as it reflects the rainfall accumulation, while tables comparing the direction of the calculated velocities and blowing wind between the proposed method and the NWP wind forecasts and the VAD derived wind components are presented. It should be noted that upper air observations are not sufficient for the observation of horizontal and vertical velocities. This is mainly because they are not very dense in time, and secondly because of the movement of the point of measurement horizontally as it ascended, making it difficult for verification of this new method (Table 1).

Separate results for direction and speed of thunderstorm movement and blowing wind are presented, as an attempt to show the differences as well as the importance of deviations between the calculated velocities and blowing wind velocities. Graphs of horizontal velocity magnitude are presented for heights ranging from surface to ~ 6.000 m (20.000 ft) comparing the proposed method and VAD results, for all times regarding the intense phenomena of each test case occurred in Figs. 5, 7, 9, 11 and 13. Direction tables are

Table 1 Table showing a summary of the five evaluation cases

Summary of evaluation cases				
Name	Description	Convection type	Area of interest	Date
TC1	Cold front	Deep	Northern Greece—Chalkidiki	Summer 2019
TC2	Cyclonic depression	Shallow	Central Greece	Autumn 2020
TC3	Deep closed cyclone	Shallow	Northern Greece	Summer 2020
TC4	Cold front	Deep	Central Greece—Attica region	Winter 2020
TC5	Thermal instability	Deep	Central Greece	Summer 2018

Table 2 Table showing for each method (VAD, model and proposed) the mean direction of horizontal velocity for time sets of 10.07.2019: (a) 1800 UTC, (b) 1900 UTC and (c) 2000 UTC

TC1 10.7.2021				
Level	Time (UTC)	Proposed	VAD 75%	Model
~910 m (3.000 ft)	1st set	290	030	280
	2nd set	290	330	190
	3rd set	290	–	200
~1500 m (5.000 ft)	1st set	290	–	290
	2nd set	290	330	290
	3rd set	290	–	290
~3000 m (10.000 ft)	1st set	280	250	280
	2nd set	290	260	290
	3rd set	290	–	280
~6.000 m (20.000 ft)	1st set	280	260	290
	2nd set	290	270	290
	3rd set	290	260	290

Table 3 Table showing for each method (VAD, model and proposed) the mean direction of horizontal velocity for time sets of 18.09.2020: (a) 0600 UTC, (b) 0700 UTC and (c) 0800 UTC

TC2 18.9.2020				
Level	Time (UTC)	Proposed	VAD 75%	Model
~910 m (3.000 ft)	1st set	130	100	070
	2nd set	140	090	060
	3rd set	250	090	070
~1500 m (5.000 ft)	1st set	140	110	070
	2nd set	150	100	070
	3rd set	250	100	090
~3000 m (10.000 ft)	1st set	160	120	110
	2nd set	220	120	110
	3rd set	120	130	100
~6.000 m (20.000 ft)	1st set	170	–	190
	2nd set	170	170	170
	3rd set	160	150	150

Table 4 Table showing for each method (VAD, model and proposed) the mean direction of horizontal velocity for time sets of 08.08.2020: (a) 1700 UTC, (b) 1800 UTC and (c) 1900 UTC

TC3 8.8.2020				
Level	Time (UTC)	Proposed	VAD 75%	Model
~910 m (3.000 ft)	1st set	100	060	350
	2nd set	350	080	350
	3rd set	100	080	360
~1500 m (5.000 ft)	1st set	090	080	040
	2nd set	080	080	050
	3rd set	100	090	050
~3000 m (10.000 ft)	1st set	080	100	080
	2nd set	090	090	080
	3rd set	090	100	080
~6.000 m (20.000 ft)	1st set	080	100	080
	2nd set	080	090	080
	3rd set	090	–	080

Table 5 Table showing for each method (VAD, model and proposed) the mean direction of horizontal velocity for time sets of 07.12.2020: (a) 0600 UTC, (b) 0700 UTC and (c) 0800 UTC

TC4 17.12.2020				
Level	Time (UTC)	Proposed	VAD 75%	Model
~910 m (3.000 ft)	1st set	260	200	160
	2nd set	120	200	160
	3rd set	230	190	210
~1500 m (5.000 ft)	1st set	260	190	170
	2nd set	230	190	170
	3rd set	250	190	190
~3000 m (10.000 ft)	1st set	240	180	190
	2nd set	260	170	180
	3rd set	240	170	170
~6.000 m (20.000 ft)	1st set	240	210	190
	2nd set	260	190	180
	3rd set	250	–	180

Table 6 Table showing for each method (VAD, model and proposed) the mean direction of horizontal velocity for time sets of 03.06.2018: (a) 1800 UTC, (b) 1900 UTC and (c) 2000 UTC. For each line, 30° are selected to identify the deviation from one method to all others

TC5 3.6.2018				
Level	Time (UTC)	Proposed	VAD 75%	Model
~910 m (3.000 ft)	1st set	300	–	270
	2nd set	350	100	300
	3rd set	290	300	310
~1500 m (5.000 ft)	1st set	300	–	320
	2nd set	330	260	300
	3rd set	320	300	310
~3000 m (10.000 ft)	1st set	310	–	330
	2nd set	340	340	340
	3rd set	320	340	350
~6.000 m (20.000 ft)	1st set	360	–	340
	2nd set	330	330	340
	3rd set	310	340	340

used to show hourly results, near the time of intense phenomena. The proposed method, VAD and model results are presented in Table 2, 3, 4, 5, 6 for heights of ~910 m, ~1.500 m, ~3.000 m and ~6.000 m (3.000 ft, 5.000 ft, 10.000 ft and 20.000 ft).

The selected convective systems that affected the Greek area represent different synoptic scale atmospheric circulation: (a) a cold front passage during summer (TC1), (b) a deep cyclonic depression (TC2), (c) an organized deep closed cyclone (TC3), (d) a cold front passage during winter (TC4) and (e) a case associated with thermally driven convective instability in summer (TC5).

Evaluation case 1: summer cold front 10.07.2019

In this case, the thunderstorm is associated with the passage of a cold front. Three days before the event, namely during the 8th of July, an upper level warm ridge was located in the area between Tunisia and Libya, with a SW-NE orientation of the ridge axis favoring low level warm advection over the Eastern Mediterranean, including the Greek area. At the same time the establishment of an upper level blocking anticyclone in the north of the Scandinavian region, operating as a dynamically unstable ridge, favored the formation of an upper level cyclone and smaller scale troughs on the eastern flank of the blocking anticyclone. During the next two days, the southern propagation of this upper level cyclone steered a surface cold front toward the southern Balkans at 10.07.2019 1200 UTC. During the period between 10.07.2019 1200 UTC and 11.07.2019 0000 UTC the edge of the surface cold front moved over northern Greece, namely over an area of a pre-existed warm advection, generating a strong 850 hPa temperature gradient over Northern Greece and a respective organized low-level cyclonic circulation, with the center over Central Macedonia. The cold front affected Northern Greece on 11.07.2019 0000 UTC. Convection promoted the formation of thunderstorms which affected Chalkidiki area (Fig. 4b), causing many human injuries and deaths as well as severe damages in the local society. Lightning activity had a peak at 1700 UTC where the system entered the Greek area until 2300 UTC. This system moved to the east, with a secondary thunderstorm following back near 2400 UTC.

For this weather event, Fig. 4a and b shows the evolution of the thunderstorm during the cold front passage over Chalkidiki area (Fig. 4b), as seen from the radars. The maximum dBz quantities are moving toward Chalkidiki area, where values over 50 and locally up to 60 dBz were measured by Thessaloniki radar. This cold front passage was very intense leading to Cumulonimbus clouds formation up to ~ 13.700 m (45.000 ft). Lines shown in Fig. 4c and d are the locations of the cross sections chosen to be presented in Fig. 4e, f and g, h, respectively. Reflectivity values over 40 dBz are located in full range of heights in this thunderstorm as shown in Fig. 4e and f.

Based on the radar information, vertical wind speed was derived with the proposed methodology. The calculated vertical velocities indicate that high positive values are located in front of the Cumulonimbus cloud, with values up to 8 m/s, as a strong indication of convectivity, that is being present and evolving through space and time. High positive values of vertical velocity also indicate the strength of the convectivity, thus being associated with extreme phenomena such as hail, intense rainfall and extreme wind gusts at surface. In addition, elevated vertical velocities values indicate that this Cumulonimbus cloud has the potential to further evolve and has not yet reached the dissipation phase. Surface

to ~ 6.000 m (20.000 ft) vertical velocity layer has a negative value of − 2 m/s, as an indication of rainfall in that area.

For this test case the wind direction derived from our method is consistent with the calculated VAD values and the modeled values, showing that directions that do not deviate more than 30° for flight levels ~ 910 m, ~ 1.500 m, ~ 3.000 m and ~ 6.000 m (3.000, 5.000, 10.000 and 20.000 ft) during 3 time periods, selected near the passage of the cold front in Chalkidiki area. Figure 5 shows a mean thunderstorm horizontal velocity ranging from 10 m/s up to 15 m/s, whereas the blowing wind has a maximum horizontal value of 55 m/s. Table 2 indicates for each line the differences between the three methods. As a reference, 30° are selected to identify the deviation from one method to all others. The green box represents that no more than 30° difference exists, whereas red box indicates a difference greater than 30° to at least one of the rest two methods.

Evaluation case 2: cyclonic depression 18.09.2020

In this case, the thunderstorms caused by a deep cyclonic depression formed on the 17th of September 2020 at 0000 UTC over the Ionian Sea in the southeast of Sicily between Italy and Greece where warm advection occurred. Surface central pressure of 993 hPa was recorded in the center of this depression. The barotropic character of the system is evident being supported by a deep upper level closed cyclone without any frontal activity at the surface. It weakened when it reached the western parts of Greece. The lightning activity was present from 0900 to 2400 UTC of 18.09.2020, where the peak was near 1200 UTC (not shown).

For this test case, Fig. 6c and d show the evolving convective weather from the upper southwest flow related to thunderstorms and Towering Cumulus clouds as well as Cumulonimbus clouds. The lack of frontal activity is related to a homogenized weather condition, where dBz are distributed up to ~ 10.600 m (35.000 ft). There are locally dBz maxima up to 40 dBz indicating isolated thunderstorms. Lines shown in Fig. 6c and d are the locations of the cross sections of Fig. 6e, f and g, h, respectively. The isolated thunderstorms that are indicated with red color ranging from 40 to 45 dBz tend to have local characteristics, as shown in the vertical cross section. Vertical velocity analysis shows that the range of positive values does not exceed 2 m/s. As a concluding remark, there is no evident deep convectivity, despite the convective character that lightning activity indicates (not shown). The future (evolution) of these thunderstorms is related to the synoptic processes being evolved.

In Table 3, a difference between the direction of movement of the thunderstorm more than 30° related to VAD and model calculated wind direction in ~ 910 m, ~ 1.500 m, ~ 3.000 m and ~ 6.000 m (3.000, 5.000, 10.000 and 20.000 ft) compared with the proposed method is shown. The model and VAD technique provide information on the wind direction
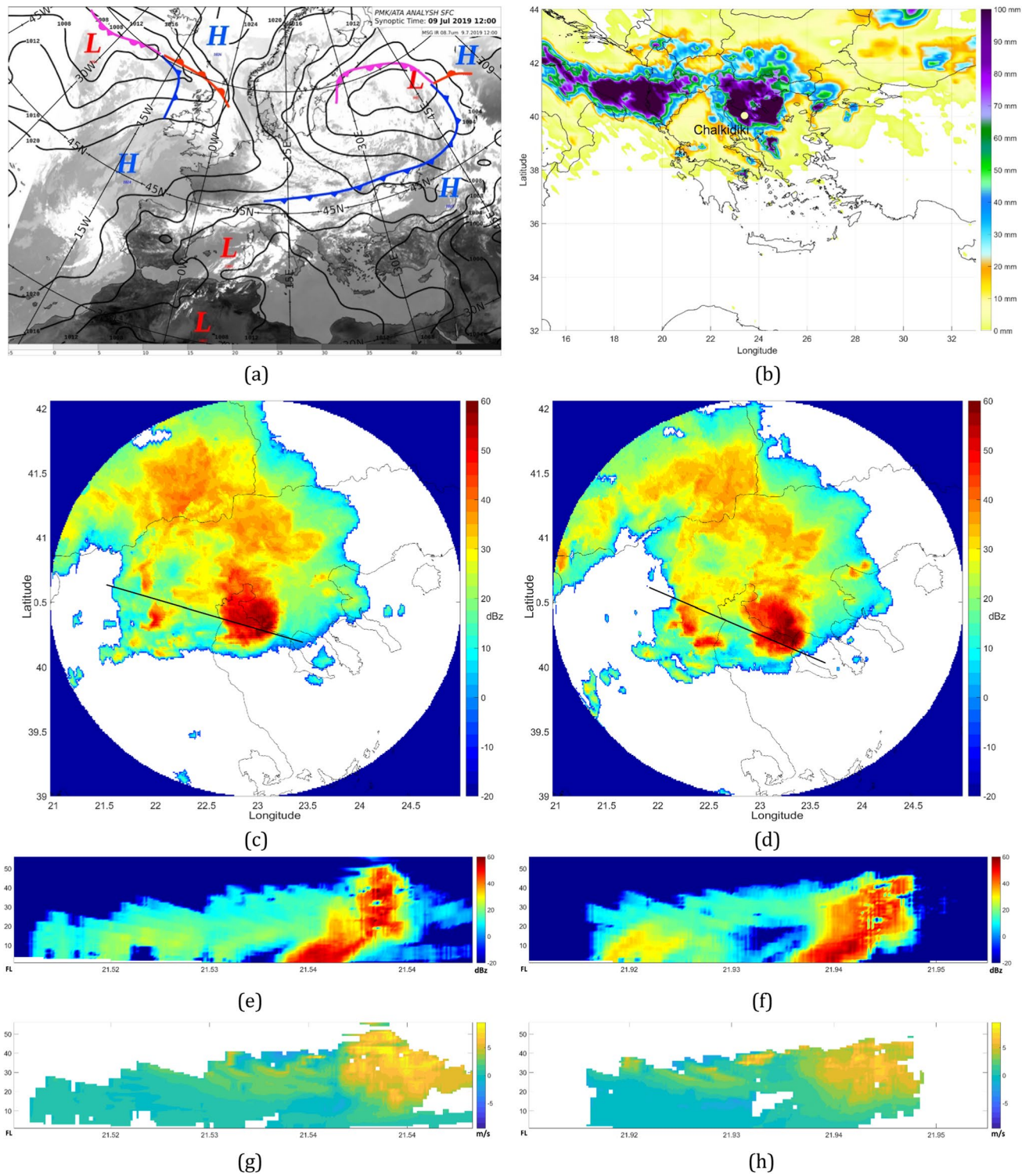
(a)

(b)

(c)

(d)

(e)

(f)

(g)

(h)

Fig. 4 **a** Surface pressure chart analysis of Europe for 09.07.2019 1200 UTC, **b** total precipitation calculated for 24 h during 10.07.2019 over Greece. Thessaloniki radar for 09.07.2019: of maximum dBz **c** at 18:32 UTC, **d** at 18:47 UTC, vertical cross section of dBz **e** at 18:32 UTC, **f** at 18:47 UTC, hybrid vertical velocity for dBz **g** at 18:32 UTC and **h** at 18:47 UTC

and its source direction. These results indicate that the thunderstorm movement is different from the blowing wind direction, showing that the direction of the thunderstorm

does not follow the path which the horizontal wind vectors have. Therefore, our method appears a great advantage compared to the other two techniques. Regarding the magnitude

Fig. 5 Mean horizontal velocity magnitude with outliers for each vertical level derived from VAD (blue) and proposed method (green) for time sets ranging from 18:02 UTC to 20:18 UTC
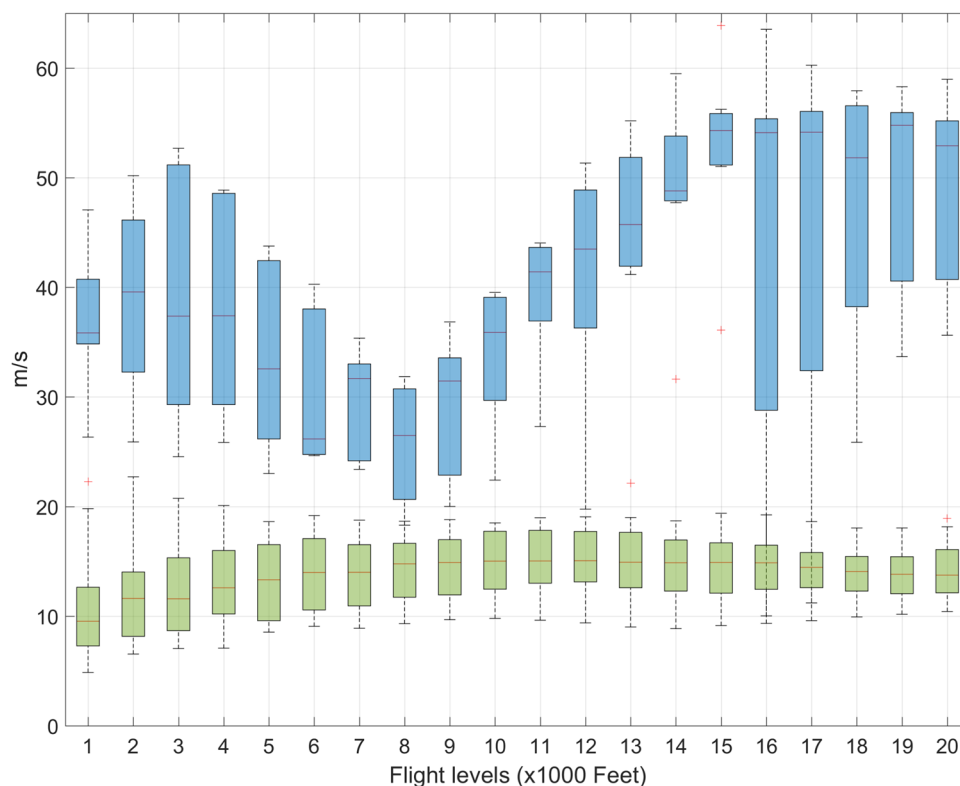
of the horizontal velocities of blowing wind and thunderstorm movement Fig. 7 indicates horizontal wind velocities of maximum 28 m/s in a descending order relative to height, whereas thunderstorm movement is characterized by a mean value of 5 m/s. Table 3 indicates for each line the differences between the three methods. As a reference, 30° are selected to identify the deviation from one method to all others. The green box represents that no more than 30° difference exists, whereas red box indicates a difference greater than 30° to at least one of the rest two methods (Fig. 7).

Evaluation case 3: deep closed cyclone 08.08.2020

An unusually organized deep closed cyclone at upper levels was established over Greece during the summer period on the 8th of August 2020, favoring large synoptic scale instability and ascending motions. The upper level system was stationary providing a large amount of precipitation especially in central and western Greece. Thunderstorm formation is evident by the lightning activity which occurred between 1600 and 2400 UTC of 08.08.2020.

Embedded Cumulonimbus clouds are evident in Fig. 8c and c where maximum dBz is shown. Thunderstorms are moving easterly affecting areas with great orographic variance. Lines shown in Fig. 8c and d are the locations of the corresponding vertical cross sections of Fig. 8e, f and g, 8h, respectively. DBz values of 40 are present with a vertical structure up to ~ 6.000 m (20.000 ft), whereas the cloud

formation reached ~ 10.600 m (35.000 ft). Vertical velocities are not high (0.5 m/s) but present, (as an indication of shallow convective system) and are located mainly in the lower levels up to ~ 6.000 m (20.000 ft).

Direction of thunderstorm movement as well as VAD and model calculated blowing wind do not derive more than 30° each with all others, except at lower levels of ~ 910 m and ~ 1.500 m (3.000 ft and 5.000 ft). Regarding the magnitude of the horizontal velocities (Fig. 9), VAD appears a maximum value of 33 m/s whereas our method estimates a mean value of 11 m/s for the thunderstorm movement. As mentioned before, Table 4 indicates for each line the differences between the three methods. As a reference, 30° are selected to identify the deviation from one method to all others. The green box represents that no more than 30° difference exists, whereas red box indicates a difference greater than 30° to at least one of the rest two methods.

Evaluation case: cold front 07.12.2020

A cold front moved eastwards from western Mediterranean and passed over Greece on the 7th of December 2020 which was a part of a large-scale frontal depression over northern Italy. The frontal depression was associated with an upper level trough being oriented from northwest to southeast facilitating the intrusion of cold air from northern Europe. This upper level trough swiped the whole Greek territory in less than 18 h: at 0000 UTC 07.12.2020. It was
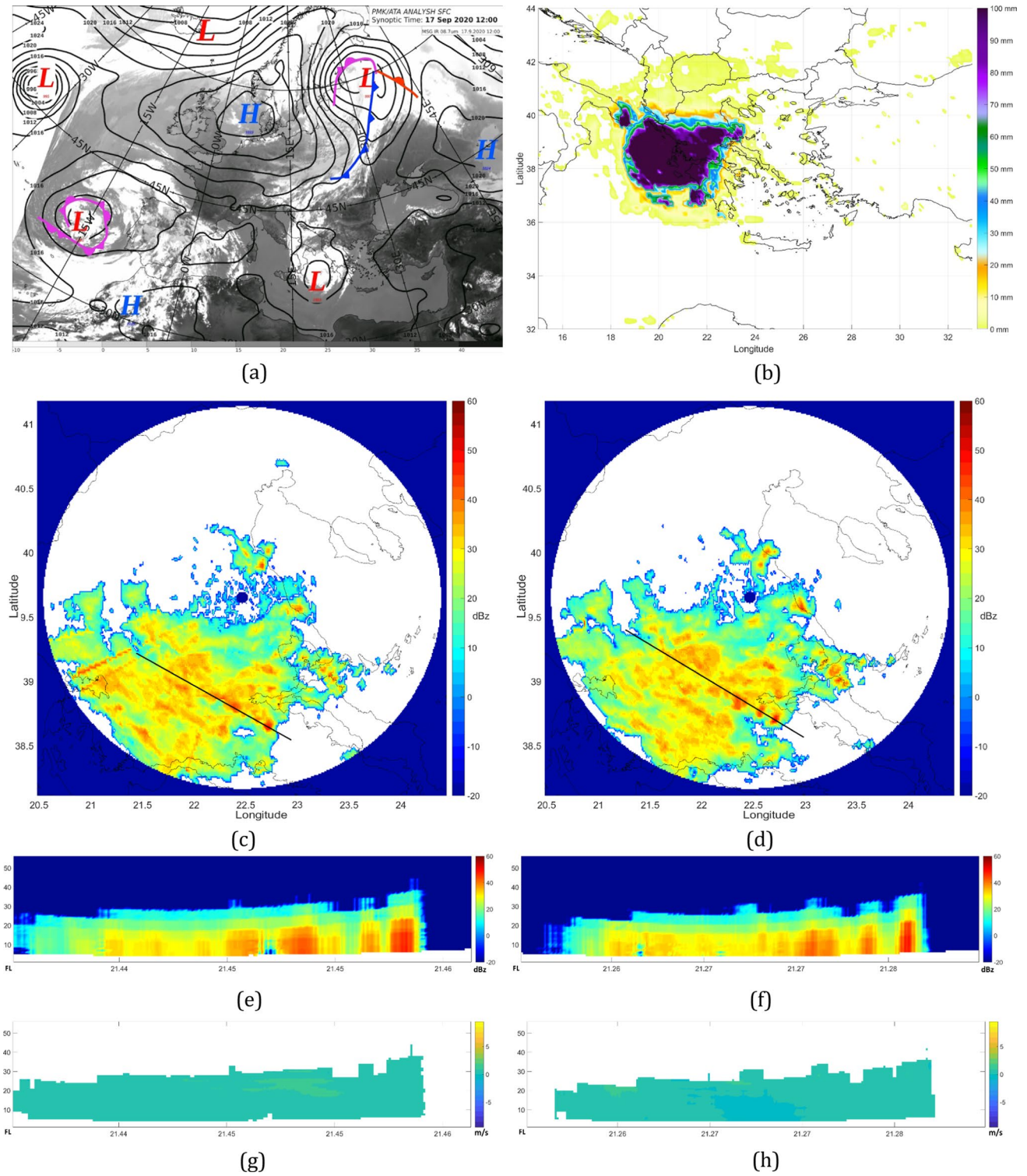
(a)

(b)

(c)

(d)

(e)

(f)

(g)

(h)

Fig. 6 **a** Surface pressure chart analysis of Europe for 17.09.2020 at 1200 UTC, **b** total precipitation calculated for 24 h for 18.09.2020 over Greece. Larissa radar for 18.09.2020: maximum dBz **c** at 0600 UTC, **d** at 06:15 UTC, vertical cross section of dBz **e** at 0600 UTC, **f**, at 06:15 UTC, hybrid vertical velocity for dBz **g** at 0600 UTC and **h** at 06:15 UTC

Fig. 7 Mean horizontal velocity magnitude with outliers for each vertical level derived from VAD (blue) and proposed method (green) for time sets ranging from 04:45 UTC to 10:15 UTC during the 18.09.2020
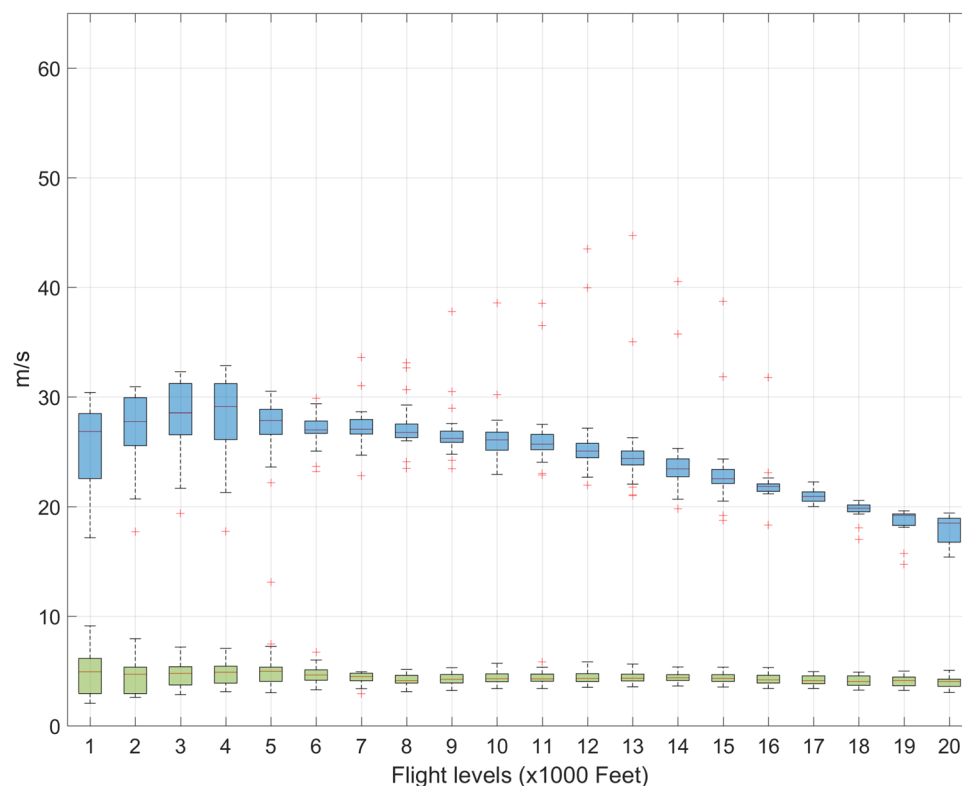
located over the Ionian Sea and over the Aegean Sea at 1800 UTC, resulting in severe weather conditions with intense phenomena of rain and gusty winds during its passage. Convective phenomena occurred over Attica between 0500 and 0900 UTC of 07.12.2020, as concluded by the lightning activity (not shown).

The VAD and model outputs reveal that the wind direction is not aligned with the thunderstorm path. Our method appears to have an advantage against NWP in this case, because it can acquire the thunderstorm movement horizontal velocity and for this reason it may be utilized for nowcasting purposes. In addition, the model predicted the thunderstorm passage with a time lag of two hours after the event (not shown).

In Fig. 10c and d, the maximum dBz is shown forming the passage of the cold front up to 35 dBz. This frontal activity was moving easterly and affected Attica region, with severe lightning activity (not shown). This test case shows some of the benefits of the proposed method, which are the capture of thunderstorm movement, as well as the high values of vertical velocities. Lines shown in Fig. 10c and d are the location of the cross sections of Fig. 10e, f and g, h, respectively. High values of vertical velocity up to 6 m/s are shown in Fig. 10e and f in front of the maximum dBz locations, where the thunderstorms are taking place, showing the future of evolving thunderstorms up to ~ 7.600 m (25.000 ft). Towering Cumulus clouds and Cumulonimbus clouds usually reach a mature stage of life which is not present at

this point and cannot be characterized as such. The dissipation of this thunderstorm is not shown, but the orographic variation is evident. It contributes to the evolution of this thunderstorm, by giving more time and intensity than usual, which is typical for Greek territory for thunderstorms and their evolution.

As shown in Table 5, both model and VAD technique correctly identified the blowing wind for this test case. Table 5 indicates for each line the differences between the three methods and 30° are selected as a reference to identify the deviation from one method to all others. The green box represents that no more than 30° difference exists, whereas red box indicates a difference greater than 30° to at least one of the other two methods. The resulting thunderstorm movement from our method showed that it is significantly different to the wind, in terms of direction; VAD and model showed a wind blowing from the south in contrast to the proposed method which showed that the thunderstorm movement approached Attica region from southwest. In the context of nowcasting, this result leads to the fact that with the applied method it is possible to estimate the arrival time of a thunderstorm at a given location, in contrast to having the VAD or model winds, which show a direction that could be confused by the thunderstorm movement. Regarding the magnitude (Fig. 11), the thunderstorm movement is no more than 10 m/s, whereas the blowing winds have a mean value of 34 m/s.
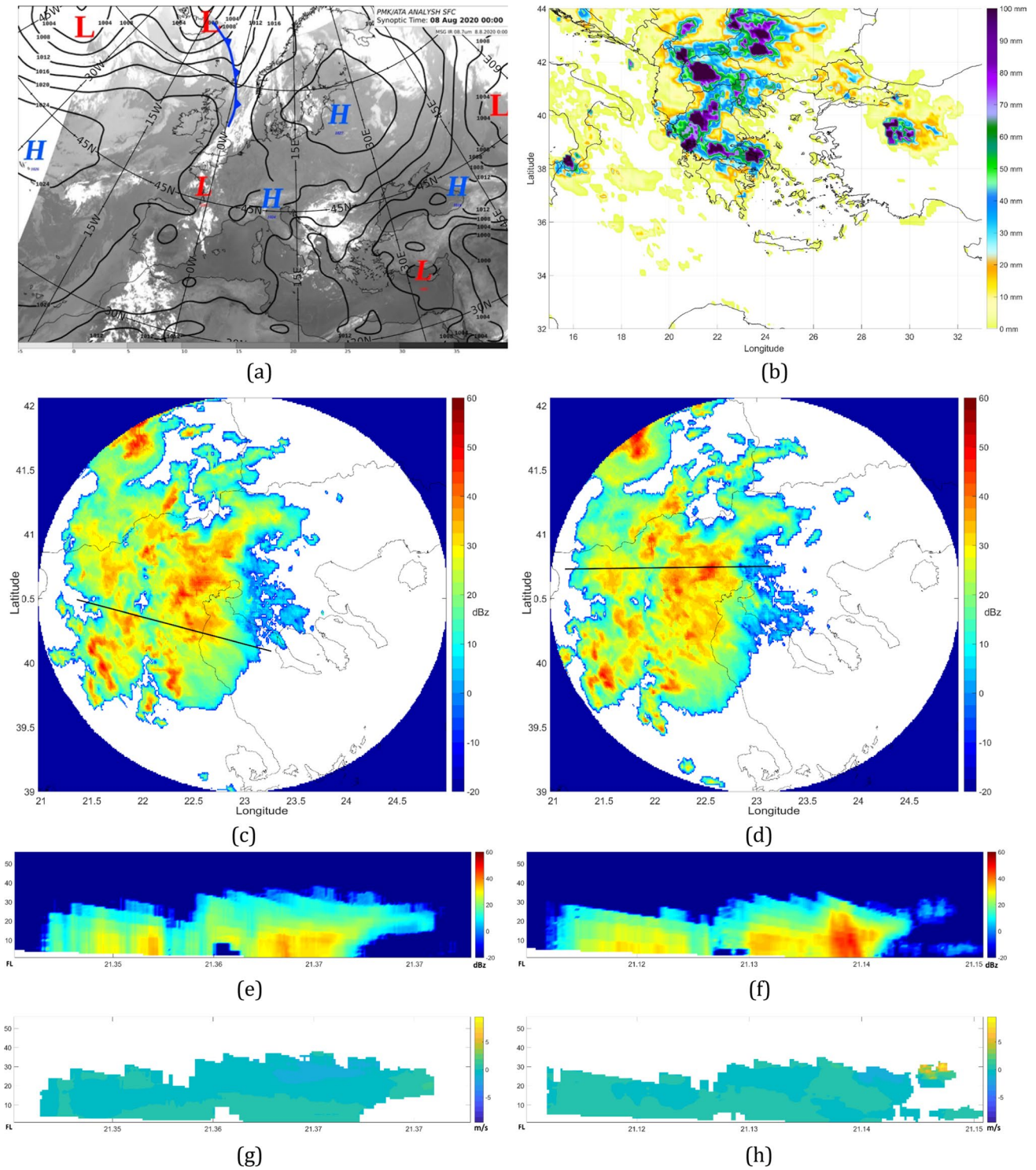
(a)

(b)

(c)

(d)

(e)

(f)

(g)

(h)

Fig. 8 **a** Surface pressure chart analysis of Europe for 08.08.2020 at 0000 UTC, **b** total precipitation calculated for 24 h during 08.08.2020 over Greece. Thessaloniki radar for 08.08.2020: maximum dBz **c** at 18:18 UTC, **d** at 18:34 UTC, vertical cross section of dBz **e** at 18:18 UTC, **f** at 18:34 UTC, hybrid vertical velocity **g** at 18:18 UTC and **h** at 18:34 UTC

Fig. 9 Mean horizontal velocity magnitude with outliers for each vertical level derived from VAD (blue) and proposed method (green) for time sets ranging from 16:59 UTC to 19:21 UTC during 08.08.2020
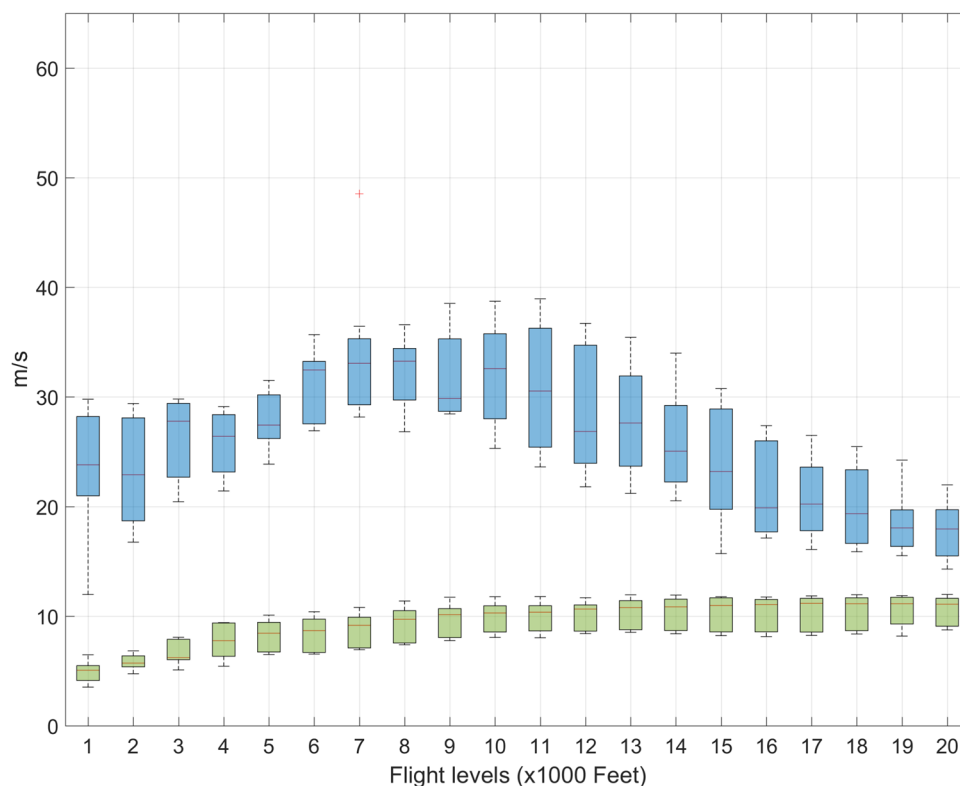
Evaluation case: thermal instability 03.06.2018

This case is associated with thermally driven convective instability in summer. On the 2nd of June 2018 north-westerly flow was established over Greece, after the passage of a trough, being followed by an anticyclone in southern west parts of the Mediterranean. At the surface, the combination of the Pakistan low with anticyclonic circulation over the Balkans resulted in northeasterly flow over the Aegean Sea, with moderate wind speeds. Warm surface temperatures favored summer convective isolated thunderstorms over the Greek land areas. During the warm hours on the 3rd of June 2018 thunderstorms occurred over Central Greece moving southwards, having a peak of the intensity of the lightning from 1700 to 2200 UTC.

Summer favors convective phenomena due to high surface temperatures and moisture in low levels of the atmosphere, resulting to thermal convection. At the test case that is evaluated, the thunderstorms as shown in Fig. 12c and d are a result of thermal convection and are characterized by slow movement in horizontal and vertical axes. High values of dBz up to 50 are present as well, in combination with electrical charges of the atmospheric field. These isolated thunderstorms developed up to ~ 10.600 m (35.000 ft). Lines shown in Fig. 12c and d are the locations of the cross section of Fig. 12e, f and

g, h, respectively. Vertical velocities exceed 2 m/s with a maximum value of 4 m/s.

The proposed method, VAD and the model results are consistent in this test case regarding the direction of the movement of the thunderstorm, having no more than 30° difference between out of any other, as shown in Table 6, a some minor exception in low altitude of ~ 910 m (3.000 ft) and for each line the differences between the three methods are highlighted. As a reference, 30° are selected to identify the deviation from one method to all others. The green box represents that no more than 30° difference exists, whereas red box indicates a difference greater than 30° to at least one of the rest two methods. These exceptions may apply due to poor radar data for evaluation, as can be shown that no 360° data (Fig. 12c, d) are present for VAD technique to be evaluated correctly. Regarding the magnitude of the blowing wind versus thunderstorm movement, the blowing wind has a maximum value of 23 m/s at 2.100 m (7.000 ft), whereas the thunderstorm movement did not exceed 7 m/s (Fig. 13).

Conclusions and discussion

The horizontal vector velocities of thunderstorm movement and the vertical hybrid velocities were estimated at different levels between 350 and 16.500 m (1.000 to 55.000 ft), for a
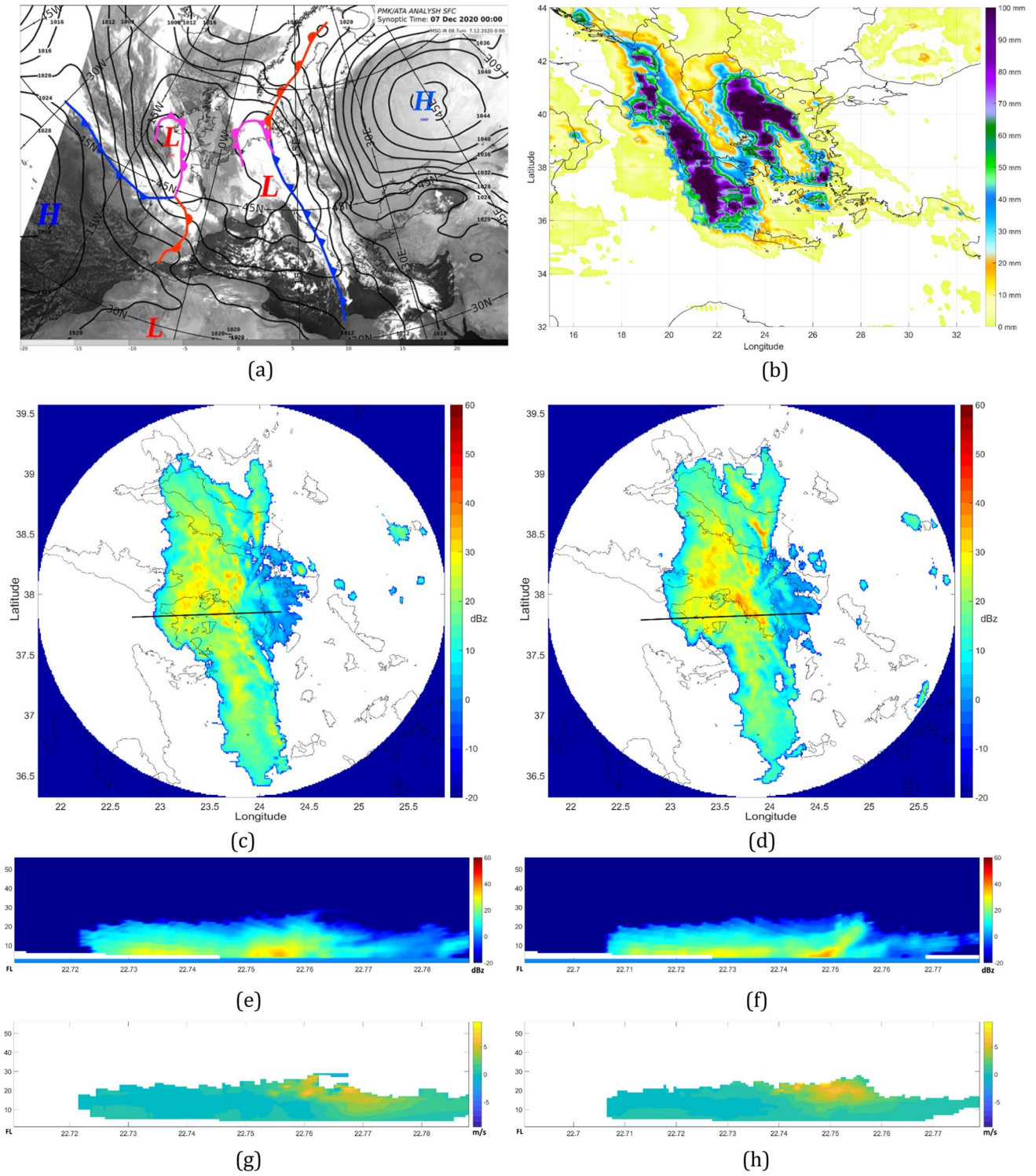
(a)

(b)

(c)

(d)

(e)

(f)

(g)

(h)

Fig. 10 **a** Surface pressure chart analysis of Europe for 07.12.2020 at 0000 UTC, **b** total precipitation calculated for 24 h during 07.12.2020 over Greece. Ymittos radar for 07.12.2020: maximum dBz **c** at 06:45 UTC, **d** at 0700 UTC, vertical cross section of dBz **e** at 06:45 UTC, **f** at 0700 UTC, hybrid vertical velocity for dBz **g** at 06:45 UTC and **h** at 0700 UTC

Fig. 11 Mean horizontal velocity magnitude with outliers for each vertical level derived from VAD (blue) and proposed method (green) for time sets ranging from 0500 UTC to 08:30 UTC during 07.12.2020
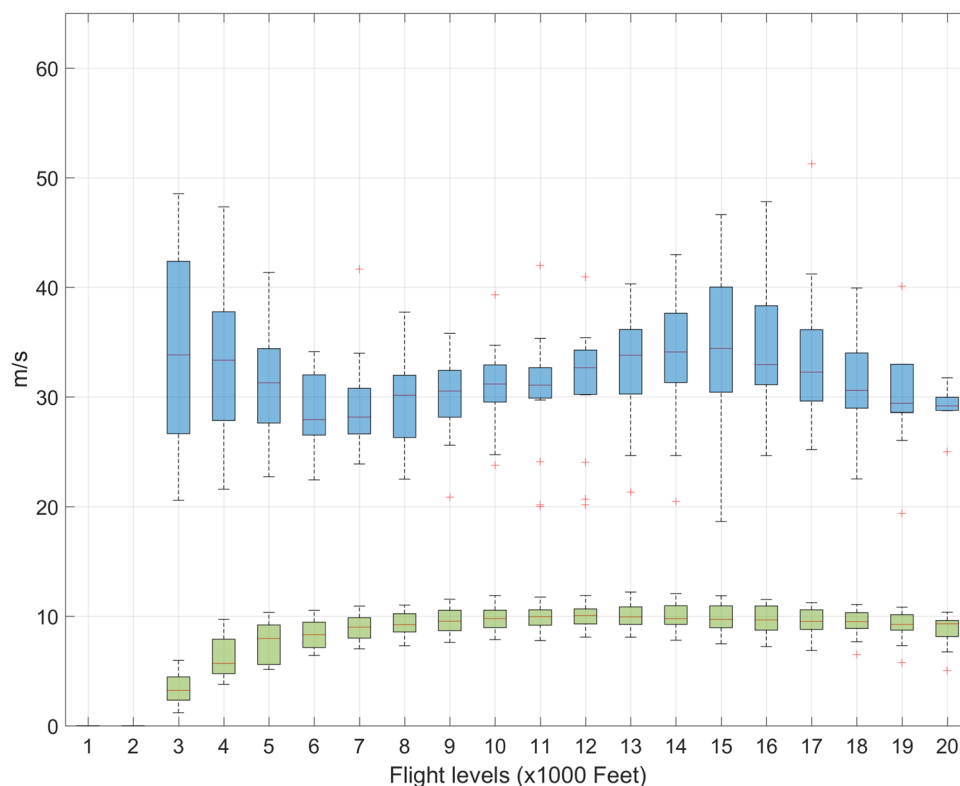
selected set of convective test cases using a novel method. The importance of this method, apart from its application in nowcasting, stands on the fact that it can derive thunderstorm movement vectors, using only the points that the radar reflectivity are present; thus can be applied for calculating wind vectors in areas with limited data and does not require a uniformly spaced area or the whole range of radar scans. In addition, with the proposed method, the results are interpolated to provide values in the missing conus area of the radar, i.e., the area with a lack of observed values over the center of the radar, resulting to a cone-shaped area gap. Wind vectors of clear sky areas are not evaluated.

In order to build the method different steps were taken for the appropriate use of the radar data.

Velocity dealiasing of Doppler weather radars is an important quality control method for data assimilation or wind field retrieval. Noise, especially when it is extended across the ray beam of radar scan, is an important factor that affects the velocity dealiasing of Doppler weather radars. A challenge in the design of dealiasing algorithms is how to effectively suppress continuous noise, using a dealiasing algorithm. This proposed method eliminates successfully clutter at all elevation levels, with respect to the initial aliased data sets. Furthermore, it could be utilized for eliminating aliasing errors regarding data assimilation techniques which require Doppler velocity.

Ray obstacles negatively impact the detection of dBz in lower scans and interpolation is not always the most effective

method for filling in missing data. A technique for filtering noisy datasets has been developed and applied with the proposed method.

Comparing our method with the VAD technique, that is widely used, our method of wind vector estimation does not require a full scan area (360°). As an example, in Fig. 2c, d, e and f as well as at TC5, our method can be applied in all areas and produce estimated velocities (where dBz measurements are present), which none of the known techniques could provide. In case of an isolated thunderstorm, our method could provide information regarding estimated arrival to specific coordinates, for a potential impact at these coordinates. In case TC4 when the thunderstorm horizontal velocity direction does not meet the direction of the atmospheric wind field (TC4), the use of the proposed method could predict more accurately the future path that a thunderstorm would move onto rather than the direction of the wind. Therefore, our method helps in monitoring thunderstorms and further in forecasting of thunderstorm life cycle and intensity.

The new method is computationally efficient and does not require the use of a supercomputer. The proposed method estimates the thunderstorm movement dislocation, whereas VAD technique enables the calculation of wind vector estimations. Therefore, the proposed method and VAD have a difference, which is proportional to the magnitude of the atmospheric winds, but also may be different depending on the synoptic weather conditions. The correlation of wind
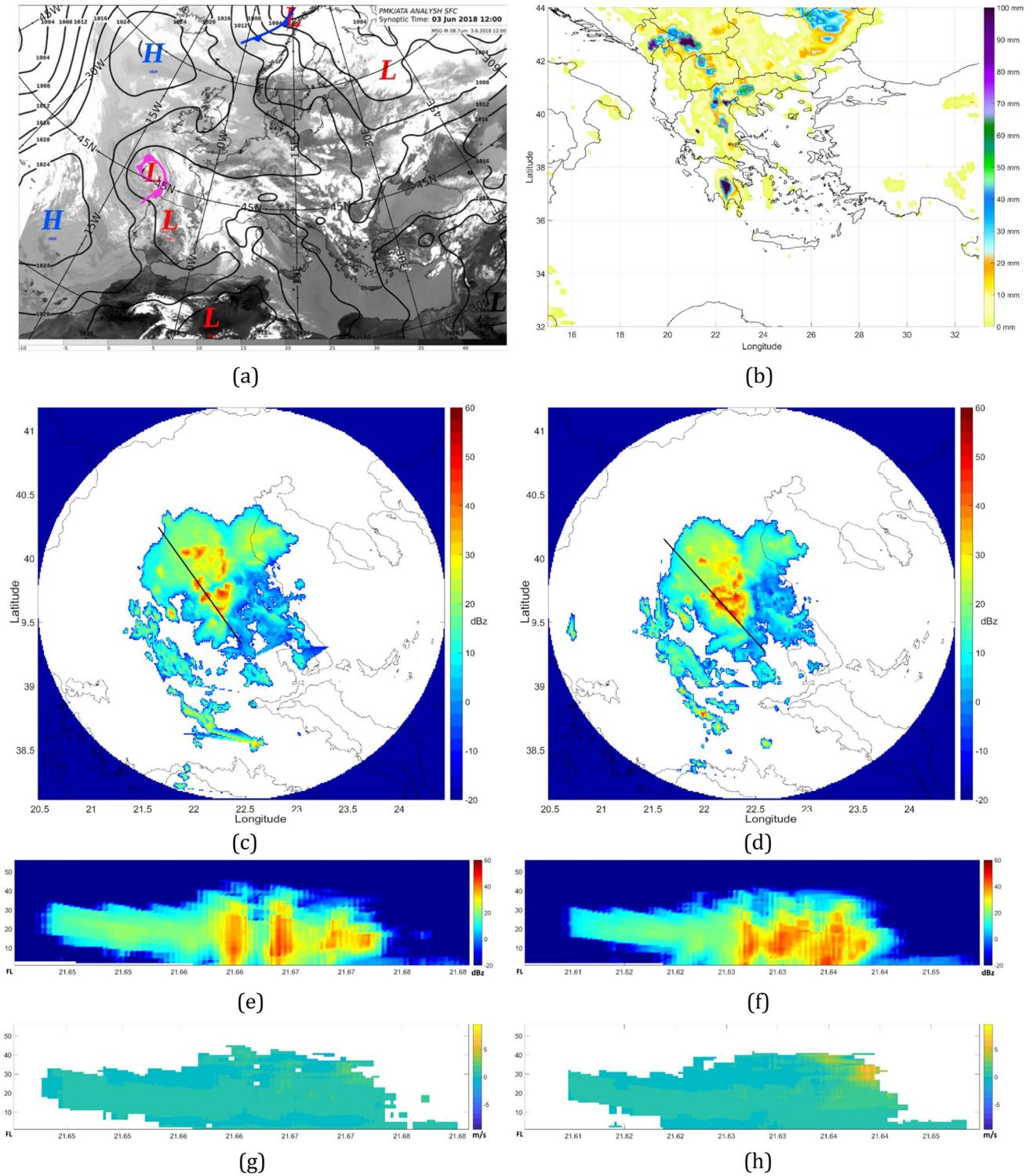
(a)

(b)

(c)

(d)

(e)

(f)

(g)

(h)

Fig. 12 **a** Surface pressure chart analysis of Europe for 03.06.2018 at 1200 UTC, **b** total precipitation calculated for 24 h during 03.06.2018 over Greece. Larissa radar for 03.06.2018: maximum dBz **c** at 18:33 UTC, **d** at 18:50 UTC, vertical cross section of dBz **e** at 18:33 UTC, **f** at 18:50 UTC, hybrid vertical velocity for dBz **g** at 18:33 UTC and **h** at 18:50 UTC

vectors and thunderstorm velocity was performed only for their direction, and a discussion was made regarding their differences in magnitude. The thunderstorm movement

calculated with the proposed method is certainly more useful than the blowing wind provided by methodologies such as VAD.

Fig. 13 Mean horizontal velocity magnitude with outliers for each vertical level derived from VAD (blue) and proposed method (green) for time sets ranging from 17:56 UTC to 20:19 UTC during 03.06.2018
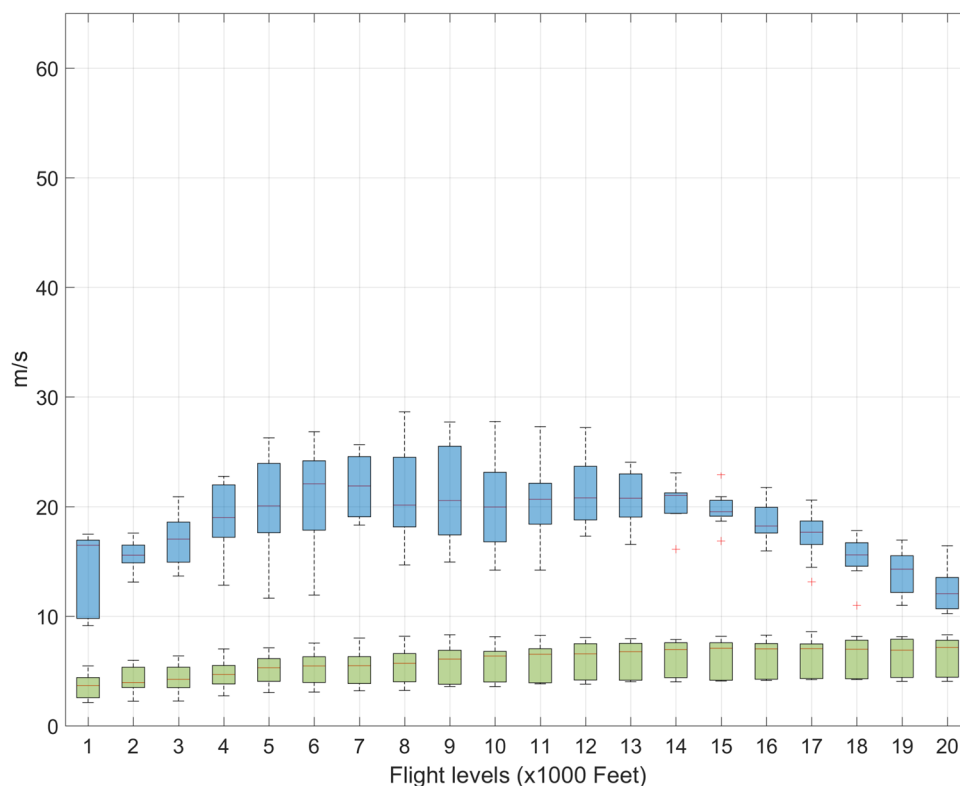
Furthermore, the estimation of vertical velocity was generally in accordance with the radar reflectivity of dBz, showing maxima where maximum convection occurred, especially when thunderstorm had its maximum intensity as shown by the maximum dBz. This additional information can also play a valuable role for nowcasting purposes. More detailed analysis of these convective weather cases can show that vertical velocity is related to dBz returns from radars, as the results of the proposed method suggest, which is an important feature for nowcasting.

Although a large number of computations is required to obtain results, the advantage of the proposed algorithm is that it does not consume computing time in an average computer more than the time required to obtain a new set of radar scans, which is less than five minutes, having the efficiency of operational usage for production. No supercomputer was used for the purposes of this paper.

The comparison of the results for the test cases showed that: (1) The horizontal velocities derived from the proposed method are the thunderstorm movement vectors, which are in general smaller in magnitude than the horizontal wind; (2) the direction of the estimated vectors versus the wind vectors can vary, dependent of the synoptic condition; where no significant upper air system exists, the direction of the winds usually tend to be very close to the proposed method; (3) the proposed method can be applied even in conditions where very few radar returns exist, while VAD technique requires a full field

of 360° scan to produce results, while the proposed method requires sequential measurements of the same radar, and (4) the application of the dealiasing and filtering methodology can yield valuable data for the assimilation of radar data.

A few major conclusions coming out from this study reflects:

- The novel method developed estimates the horizontal vector velocities of thunderstorm movement and vertical hybrid velocities using radar reflectivities. It can be applied in areas with limited data and does not require uniformly spaced area data or the complete range of radar scans.
- A successful clutter elimination was demonstrated, enhancing the quality of Doppler weather radar for data assimilation and wind field retrieval purposes.
- The method developed includes a technique for filtering noisy datasets, thereby for overcoming, in a great percentage, the challenges of continuous noise and ray obstacles.
- Compared to the widely used VAD technique and NWP results, the new method can provide estimates even in areas with partial scan coverage and can predict the future path of a thunderstorm more accurately.
- The method shows a correlation between thunderstorm movement and wind vectors and proves to be more use-

ful for nowcasting purposes than existing methodologies such as VAD.

- The estimation of vertical velocity aligns with radar reflectivity values, indicating areas of convection.

Declarations

Conflict of interest On behalf of all authors, the corresponding author states that there is no conflict of interest.

References

Battan LJ (1973) Radar observation of the atmosphere. Quart J R Meteorol Soc 99(422):793–793. https://doi.org/10.1002/qj.49709942229

Browning KA, Wexler R (1968) The Determination of Kinematic Properties of a Wind Field Using Doppler Radar. J Appl Meteorol 7(1):105–113. https://doi.org/10.1175/1520-0450(1968)007%3c0105:tdokpo%3e2.0.co;2

Cassola F et al (2023) Extreme convective precipitation in Liguria (Italy): a brief description and analysis of the event occurred on October 4, 2021. Bull Atmos Sci Technol. https://doi.org/10.1007/s42865-023-00058-3

Chan SH et al (2010) Subpixel motion estimation without interpolation. In: 2010 IEEE international conference on acoustics speech and signal processing https://doi.org/10.1109/icassp.2010.5495054

Divjak M (1999) Radar data quality-ensuring procedures at european weather radar stations. Eumetnet Opera Programme https://diameter.si/research/radqual.pdf

Dudhia J (1989) Numerical study of convection observed during the winter monsoon experiment using a mesoscale two-dimensional model. J Atmos Sci 46(20):3077–3107. https://doi.org/10.1175/1520-0469(1989)046%3c3077:nsocod%3e2.0.co;2

Eilts MD, Smith SD (1990) Efficient dealiasing of doppler velocities using local environment constraints. J Atmos Ocean Technol 7(1):118–128. https://doi.org/10.1175/1520-0426(1990)007%3c0118:edodvu%3e2.0.co;2

Gastaldo T et al (2018) Data assimilation of radar reflectivity volumes in a LETKF scheme. Nonlinear Process Geophys 25:747–764. https://doi.org/10.5194/npg-25-747-2018

Honda T et al (2022a) Development of the real-time 30-s-update big data assimilation system for convective rainfall prediction with a phased array weather radar: description and preliminary evaluation. J Adv Model Earth Syst. https://doi.org/10.1029/2021ms002823

Hong SY, Lim JOJ (2006) The WRF single-moment 6-class microphysics scheme (WSM6). Asia-Pac J Atmos Sci 42(2):129–151

Hong SY et al (2006) A new vertical diffusion package with an explicit treatment of entrainment processes. Mon Weather Rev 134(9):2318–2341. https://doi.org/10.1175/mwr3199.1

Huffman GJ et al (2020) Integrated multi-satellite retrievals for the global precipitation measurement (GPM) mission (IMERG). Advances in global change research. Springer International Publishing, Berlin, pp 343–353. https://doi.org/10.1007/978-3-030-24568-9_19

Kain JS (2004) The Kain fritsch convective parameterization: an update. J Appl Meteorol 43(1):170–181. https://doi.org/10.1175/1520-0450(2004)043%3c0170:tkcpau%3e2.0.co;2

Liu Y et al (2021) Assimilation of doppler weather radar data with a regional WRF-3DVAR system: influence of data assimilation volume on precipitation forecast. In: 2021 IEEE international geoscience and remote sensing symposium IGARSS, Brussels, Belgium, pp 7091–7094, https://doi.org/10.1109/IGARSS47720.2021.9554143

Lee WC et al (2014) Distance velocity-Azimuth display (DVAD)—new interpretation and analysis of doppler velocity. Mon Weather Rev 142:573–589. https://doi.org/10.1175/MWR-D-13-00196.1

Li N, Wei M (2010) An automated velocity dealiasing method based on searching for zero isodops. Quart J R Meteorol Soc 136(651):1572–1582. https://doi.org/10.1002/qj.664

Liang X (2007) An integrating velocity Azimuth process single-doppler radar wind retrieval method. J Atmos Ocean Technol 24(4):658–665. https://doi.org/10.1175/jtech2047.1

Liang X et al (2019) An IVAP-based dealiasing method for radar velocity data quality control. J Atmos Ocean Technol 36:2069–2085. https://doi.org/10.1175/JTECH-D-18-0216.1

Lim HC, Lee DI (2009) A comparative analysis of two wind velocity retrieval techniques by using a single doppler radar. Hydrol Earth Syst Sci 13(5):651–661. https://doi.org/10.5194/hess-13-651-2009

Luo ZJ et al (2014) Convective vertical velocity and cloud internal vertical structure: an a-train perspective. Geophys Res Lett 41(2):723–729. https://doi.org/10.1002/2013gl058922

Nair MR et al (2022) Remote sensing of vertical wind for the characterization of atmospheric convection. In: URSI regional conference on radio science (USRI-RCRS), Indore, India, pp 1–5, https://doi.org/10.23919/URSI-RCRS56822.2022.10118514

Nolan DS et al (2021) Evaluation of the surface wind field over land in WRF simulations of Hurricane Wilma (2005). Part II: surface winds, inflow angles, and boundary layer profiles. Mon Weather Rev 149:697–713. https://doi.org/10.1175/MWR-D-20-0201.1

Persson P (1987) A real-time system for automatic Single-Doppler wind field analysis. In: Proceedings of the symposium on mesoscale analysis and forecasting, Vancouver, BC, Canada, ESA, 61–66.

Powers-NCAR/UCAR (2008) A description of the advanced research WRF Version 3. NCAR UCAR. https://doi.org/10.5065/D68S4MVH

Rinehart RE (2004) Radar for meteorologists, 4th edn. Rinehart Publishing

Šaur D et al (2021) Radar and station measurement tresholds for more accurate forecast of convective precipitation. In: 2021 International conference on military technologies (ICMT), Brno, Czech Republic, pp 1–7 https://doi.org/10.1109/ICMT52455.2021.9502811

Sawyer JS (1977) The ceaseless wind. By John A. Dutton. McGraw-Hill New York and London. In: Quarterly Journal of the Royal Meteorological Society, vol 103, No 436, pp 376–376. Wiley. https://doi.org/10.1002/qj.49710343615

Shelekhova EA et al (2010) Simulation of doppler lidar measurements using the WRF and Yamada-Mellor models, In: Proceedings of SPIE 7832, Lidar technologies, techniques, and measurements

for atmospheric remote sensing VI, 783205, https://doi.org/10.1117/12.864840

Skolnik MI (2008) Radar handbook, 3rd edn. McGraw-Hill, New York

Sugimoto et al (2009) An examination of WRF 3DVAR radar data assimilation on its capability in retrieving unobserved variables and forecasting precipitation through observing system simulation experiments. Mon Weather Rev 137(11):4011–4029. https://doi.org/10.1175/2009mwr2839.1

Tao Z (1992) The vap method to retrieve the wind vector field based on single-doppler velocity field. Acta Meteorol Sin. https://doi.org/10.11676/qxxb1992.009

Tian L et al (2015) Velocity–azimuth display analysis of Doppler velocity data for HIWRAP. J Appl Meteor Climatol 54:1792–1808. https://doi.org/10.1175/JAMC-D-14-0054.1

Waldteufel P, Corbin H (1979) On the analysis of single-doppler radar data. J Appl Meteorol 18(4):532–542. https://doi.org/10.1175/1520-0450(1979)018%3c0532:otaosd%3e2.0.co;2

Wan F et al (2021) Supercell storm and extreme wind in a linear mesoscale convective system. In: 2021 IEEE 23rd interantional conference on high performance computing and communications; 7th interantional conference on data science and systems; 19th interantional conference on smart city; 7th interantional conference on dependability in sensor, cloud and big data systems and application, Haikou, Hainan, China, pp 2264-2269, https://doi.org/10.1109/HPCC-DSS-SmartCity-DependSys53884.2021.00339